**Climate
of the Past**

NALPS: a precisely dated European climate record 120–60 ka

R. Boch[1,2]**, H. Cheng**[2,3]**, C. Spötl**[1]**, R. L. Edwards**[2]**, X. Wang**[2,4]**, and Ph. Häuselmann**[5]

[1]Institut für Geologie und Paläontologie, Universität Innsbruck, Austria
[2]Department of Geology and Geophysics, University of Minnesota, Minneapolis, USA
[3]Institute of Global Environmental Change, Xi'an Jiaotong University, Xi'an, China
[4]Lamont-Doherty Earth Observatory of Columbia University, Palisades, NY, USA
[5]Swiss Institute of Speleology and Karst Sciences – SISKA, La Chaux-de-Fonds, Switzerland

Abstract. Accurate and precise chronologies are essential in understanding the rapid and recurrent climate variations of the Last Glacial – known as Dansgaard-Oeschger (D-O) events – found in the Greenland ice cores and other climate archives. The existing chronological uncertainties during the Last Glacial, however, are still large. Radiometric age data and stable isotopic signals from speleothems are promising to improve the absolute chronology. We present a record of several precisely dated stalagmites from caves located at the northern rim of the Alps (NALPS), a region that favours comparison with the climate in Greenland. The record covers most of the interval from 120 to 60 ka at an average temporal resolution of 2 to 22 yr and 2σ-age uncertainties of ca. 200 to 500 yr. The rapid and large oxygen isotope shifts of 1 to 4.5 ‰ occurred within decades to centuries and strongly mimic the Greenland D-O pattern. Compared to the updated Greenland ice-core timescale (GICC05modelext) the NALPS record confirms the timing of rapid warming and cooling transitions between 118 and 106 ka, but suggests younger ages for D-O events between 106 and 60 ka. As an exception, the timing of the rapid transitions into and out of the stadial following GI 22 is earlier in NALPS than in the Greenland ice-core timescale. In addition, there is a discrepancy in the duration of this stadial between the ice-core and the stalagmite chronology (ca. 2900 vs. 3650 yr). The short-lived D-O events 18 and 18.1 are not recorded in NALPS, provoking questions with regard to the nature and the regional expression of these events. NALPS resolves recurrent short-lived climate changes within the cold Greenland stadial and warm interstadial successions, i.e. abrupt warming events preceding GI 21 and 23 (precursor-type events) and at the end of GI 21 and 25 (rebound-type events), as well as intermittent cooling events during GI 22 and 24. Such superimposed events have not yet been documented outside Greenland.

1 Introduction

In the Greenland ice cores drastic climate changes are documented during the Last Glacial period. The rapid and recurrent variations – known as Dansgaard-Oeschger (D-O) events (Dansgaard et al., 1993; Grootes et al., 1993) – are expressed as relatively warm and humid Greenland Interstadials (GI) and relatively cold and dry Greenland Stadials (GS; see Rousseau et al., 2006; Lowe et al., 2008 for an event-stratigraphical recommendation). These successions had a global effect on climate (e.g. Clement and Peterson, 2008). Large and rapid air temperature changes occurred within a few years to a few decades (Steffensen et al., 2008). The amplitude was largest in the N-Atlantic realm and reached 8–16 °C during rapid warmings in Greenland (Severinghaus et al., 1998; Lang et al., 1999; Huber et al., 2006; Capron et al., 2010). The millennial-scale changes also affected the concentration of greenhouse gases (Grachev et al., 2007; Loulergue et al., 2008), as well as global sea-level and high-latitude ice-sheets (Lambeck and Chappell, 2001; Arz et al., 2007). Recently, the occurrence of three types

of short-lived, sub-millennial climate events was discussed (Capron et al., 2010). These events occurred within D-O cycles and consist of abrupt warmings either preceding individual GI (named precursor events) or occurring toward the end of some of the GI (named rebound events), as well as of abrupt coolings, e.g. during GI 24 (Capron et al., 2010).

The D-O variations show a quasi-periodic occurrence of ca. 1470 yr (Bond et al., 1997; Grootes and Stuiver, 1997; Rahmstorf, 2003), although a recent study suggested that the recurrence interval is not robust and thus not significant (Peavoy and Franzke, 2010). Different triggers and mechanisms have been invoked to explain these rapid climate changes. Among these are freshwater influx into the North Atlantic (Clark et al., 2001; Arz et al., 2007), solar variations (e.g. Braun et al., 2005), internal oscillations (Broecker et al., 1990; Birchfield et al., 1994; Rahmstorf, 2002) and stochastic resonance (Alley et al., 2001; Claussen et al., 2003; Ditlevsen and Johnsen, 2010). Moreover, changes and different states of the Atlantic Meridional Overturning Circulation (AMOC) are discussed as internal forcings (Ahn and Brook, 2008; Schmittner and Galbraith, 2008), including latitudinal shifts in the location of North Atlantic Deep Water production (e.g. Ganopolski and Rahmstorf, 2002). Others claim a tropical trigger of the D-O variability (Clement and Cane, 1999; Clement and Peterson, 2008), or a rapidly changing windfield due to the dynamics of continental ice sheets (Wunsch, 2006). Ditlevsen and Johnsen (2010) recently reported evidence that internal noise triggered D-O warmings and concluded that these events cannot be predicted.

Accurate and precise chronologies are fundamental to improve our understanding of the enigmatic D-O pattern and its global teleconnections. The existing chronological uncertainties during the Last Glacial, however, are still significant (Svensson et al., 2008) and various timescales are available for Greenland ice cores alone (Meese et al., 1997; Johnsen et al., 2001; Svensson et al., 2008; Wolff et al., 2010). The multi-parameter, annual layer-counted GICC05 timescale (Svensson et al., 2008) covers the past 60 kyr and age uncertainties are on the order of 2.5 kyr at 60 ka. For the first half of the Last Glacial (ca. 118–60 ka) the GICC05modelext timescale (Wolff et al., 2010) was recently suggested as an improvement of the previous ss09sea timescale (North Greenland Ice Core Project members, 2004). A comparison of the ice-core chronologies with those from other Last Glacial archives, e.g. N-Atlantic deep-marine sediments, suffers from the radiocarbon dating limit and uncertainties associated with the ^{14}C-calibration and the marine reservoir effect. U-Th-dated speleothem chronologies are promising and help to reduce the dating uncertainties substantially. Previous studies showed that speleothems capture the D-O pattern and provide valuable contributions (e.g. Wang et al., 2001, 2007, 2008; Spötl et al., 2006; Genty et al., 2003; Cruz et al., 2005; Dykoski et al., 2005; Drysdale et al., 2007; Cheng et al., 2009; Fleitmann et al., 2009; Asmerom et al., 2010).

In the Alps, which are known to be a climatically sensitive region (Casty et al., 2005; Auer et al., 2007), the speleothem O isotopic composition constitutes a climate proxy that allows for a direct comparison with the Greenland O isotope records (e.g. von Grafenstein et al., 1999; Spötl and Mangini, 2002). In particular, the Alps and Greenland share a dominant Atlantic influence and the common O isotopic signal allows comparison of the chronology of the ice-cores to that of radiometrically dated speleothems.

In this study we present a record consisting of several precisely dated stalagmites from caves located at the northern rim of the European Alps (NALPS). This region is exposed to a strong Atlantic influence via northwesterly winds thus favouring a comparison with climate in Greenland. Moreover, the cave host rock favours deposition of speleothems with excellent geochemical dating characteristics. All Last Glacial samples exhibit sharp O isotope transitions highly reminiscent of the D-O pattern seen in the ice cores. Our record covers most of the first half of the Last Glacial period (118–64 ka) at high temporal resolution.

2 Cave sites and stalagmite samples

Four cave sites were selected for this study (Fig. 1). Beatus Cave is located in central Switzerland and samples were collected in a gallery at 875 m a.s.l. The cave air temperature is ca. 8 °C and mean annual precipitation is 1258 mm (2004–2008; meteorological station Interlaken, ca. 8 km from the cave). Baschg Cave is located in the westernmost part of Austria and the cave entrance is at 780 m a.s.l. The cave air temperature is ca. 10 °C and mean annual precipitation is 1231 mm (1971–2000; meteorological station Feldkirch, ca. 5 km from the cave). Klaus-Cramer and Schneckenloch Caves are located close to each other on the margin of the high-alpine Gottesacker karst plateau in western Austria (Fig. 1). Klaus-Cramer Cave is a shallow cave and the entrance opens at 1964 m a.s.l. The cave air temperature is only ca. 1–2 °C. The entrance of Schneckenloch Cave is at ca. 1270 m and the cave air temperature is ca. 6.5 °C. Mean annual precipitation at both sites is 1908 mm (1971–2000; station Schoppernau, 835 m a.s.l. and ca. 7 km from the caves). All four caves have small and well-defined catchments (a few km^2 only) and developed in the same carbonate host rock (Lower Cretaceous Schrattenkalk Formation). This host rock provides favourable geochemical conditions for U-Th dating, i.e. high U (0.5–2 ppm) and low detrital Th concentrations (typically 0.2–6 ppb [232]Th). Therefore, no significant correction of the U-Th ages is needed and the resulting ages are precise and accurate. Two stalagmites were recovered from Beatus, three from Baschg, one from Klaus-Cramer, and one from Schneckenloch Cave. Some samples were found broken while others were still in growth position. The stalagmites are typically small in size, i.e. between 11 and 38 cm high and near-equal in diameter
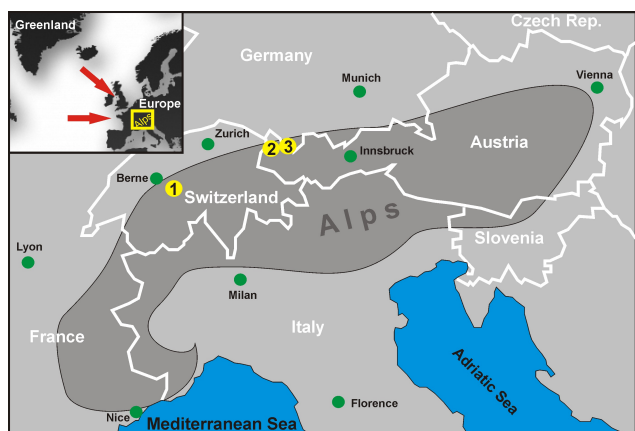
Fig. 1. Location of the selected cave sites at the northern rim of the Alps: **(1)** Beatus Cave (Switzerland); **(2)** Baschg Cave (Austria); **(3)** Klaus-Cramer- and Schneckenloch Caves (Austria). The northern rim of the Alps is dominated by moisture advection from the Atlantic Ocean (red arrows).

along their growth axes. The samples consist of dense calcite and some show distinct lamination. Minor portions of some samples (typically near the base) consist of impure calcite due to clay and organic inclusions. These sections were not used in the combined record. Interestingly, speleothem growth locally also occurred during cold stadial conditions. This places tight constraints on the minimum temperatures of these alpine caves.

3   Methods

The stalagmites were cut in half and a 0.5 to 1 cm-thick slab was cut from the axial part and polished. Subsamples for radiometric U-Th dating (typically 0.05 to 0.1 g) were obtained using a dentist drill. After dissolving the powders in nitric acid and adding a mixed ^{229}Th-^{233}U-^{236}U spike, U and Th were separated from each other and from matrix elements using co-precipitation with Fe and an ion-exchange resin in Teflon columns (procedure similar to Edwards et al., 1986). The isotopic compositions of U and Th of the majority of the samples were analysed using a ThermoFinnigan NEPTUNE multi-collector inductively-coupled plasma mass spectrometer (MC-ICP-MS; Cheng et al., 2009). The remaining samples were analysed on a ThermoFinnigan ELEMENT single-collector ICP-MS (Shen et al., 2008). In both cases a spiked NBL-112A standard solution was measured before and after the sample runs and blank measurements were conducted to correct for the U and Th backgrounds. Isotopic activity ratios were calculated using the new decay constants of Cheng et al. (2008). The final ages were corrected for detrital Th using an initial ^{230}Th/^{232}Th activity ratio of 0.8 (cf. Richards and Dorale, 2003). Ages are quoted in "a BP" (years before 1950 A.D.; see Table 1). The U-Th-based age models (cf. Fig. S1

in the Supplement) were calculated using the open-source R statistics software (version 2.10.0; R Development Core Team, 2010) and an algorithm optimised for speleothems (Scholz and Hoffmann, 2011). The age-depth function and the corresponding 95 %-confidence intervals were calculated by superposition of ensembles of piecewise linear fits. In addition to the U-Th data points and corresponding errors the algorithm also uses stratigraphic information, i.e. the age of the speleothem must increase with increasing distance from top.

Stalagmite slabs and thin sections were investigated using transmitted-light, epifluorescence, as well as reflected-light microscopy. Subsamples for stable oxygen and carbon isotopic analysis were micromilled at 0.15 to 0.25 mm resolution along the central stalagmite growth axes. The isotopic compositions were analysed using a ThermoFisher Delta^{plus}XL isotope ratio mass spectrometer coupled to a ThermoFisher GasBench II. Results are reported relative to the VPDB standard and the precision of the δ^{18}O and δ^{13}C values is 0.08 and 0.06 ‰ (1-sigma), respectively (Spötl and Vennemann, 2003). In this paper, we focus on the palaeoclimatic application of the O isotopic signal.

4   The NALPS stalagmite record

The new O isotope record from the northern Alps covers the time interval from ca. 120 to 60 ka, i.e. D-O 25 to D-O 18 (data are available in the Supplement). Interstadials dominate the record, reflecting favourable climate conditions with regard to speleothem growth. Speleothem formation, however, continued at least during some of the stadials, indicating that the caves were not frozen during these times. The record from seven stalagmites is temporally constrained by 154 U-Th ages (20–30 per stalagmite; Table 1). Typical relative 2σ-uncertainties range from 0.2–0.6 %, i.e. average uncertainties associated with the timing and duration of rapid climate changes range from ca. 200 to 500 yr (stalagmites KC1 210 yr, BA1-clean section 410 yr, BA1b 350 yr, BA2 340 yr, EXC3 450 yr, EXC4 400 yr, SCH7 530 yr; cf. Fig. 2).

The NALPS stable isotope curves consist of ca. 8200 individual analyses and show rapid and large isotope shifts of up to 4.5 ‰ underscoring the high sensitivity of these cave sites. The average temporal resolution ranges from 2 to 22 yr depending on the stalagmite and time interval. With regard to the transitions, a sharp (rapid) central portion is often flanked by more gradual progressions towards the isotopic maxima and minima. This could either be an expression of the regional climate, reflect hydrological processes in the karst aquifer, or could in part be a smoothing artefact of the applied age model. Regarding the climatic interpretation of the alpine speleothem O isotopic signal, the pattern is highly reminiscent of Greenland, i.e. high δ^{18}O values represent warm interstadials and low values cold stadials (Fig. 2). The speleothem O isotope values primarily

Table 1. U-Th dating results of seven stalagmites from four cave sites.

Sample	^{238}U [ppb]	^{232}Th [ppt]	^{230}Th/^{232}Th [atomic x10^{-6}]	δ^{234}U[a] [measured]	^{230}Th/^{238}U [activity]	Age [a] [uncorr.]	Age [a] [corr.]	δ^{234}U[b]$_{Initial}$ [corr.]	Age [a BP][c] [corr.]	DFT [mm][d] isotrack-scale
KC1-0.1	224.5 ±0.3	3920 ±80	830 ±20	1142.0 ±3.0	0.8800 ±0.0020	54 840 ±190	54 620 ±250	1332.0 ±3.0	54 560 ±250	1.0
KC1-0.2	294.1 ±0.3	1310 ±30	3320 ±70	1084.0 ±2.0	0.8980 ±0.0020	58 240 ±150	58 180 ±160	1277.0 ±3.0	58 120 ±160	2.3
KC1-0.5	334.0 ±1.0	580 ±10	8660 ±120	1090.0 ±8.0	0.9130 ±0.0050	59 290 ±480	59 260 ±480	1289.0 ±9.0	59 200 ±480	4.5
KC1-0.8	415.2 ±0.3	640 ±10	9840 ±200	1013.0 ±2.0	0.9220 ±0.0020	63 100 ±140	63 080 ±140	1211.0 ±3.0	63 020 ±140	7.5
KC1-1.0	463.0 ±1.0	470 ±10	14 830 ±300	990.0 ±2.0	0.9190 ±0.0020	63 830 ±160	63 820 ±160	1185.0 ±2.0	63 760 ±160	9.8
KC1-2.0	536.0 ±1.0	142 ±3	57 360 ±1300	984.0 ±2.0	0.9220 ±0.0020	64 300 ±160	64 300 ±160	1179.0 ±2.0	64 240 ±160	19.5
KC1-3.0	607.0 ±1.0	420 ±10	21 850 ±450	981.0 ±2.0	0.9260 ±0.0020	64 750 ±170	64 750 ±170	1178.0 ±3.0	64 690 ±170	30.0
KC1-4.5	485.0 ±0.4	1040 ±20	7240 ±150	971.0 ±2.0	0.9380 ±0.0010	66 350 ±150	66 330 ±150	1170.0 ±3.0	66 270 ±150	45.0
KC1-6.0	565.0 ±1.0	240 ±10	36 610 ±760	972.0 ±2.0	0.9510 ±0.0010	67 550 ±190	67 540 ±190	1176.0 ±3.0	67 480 ±190	60.0
KC1-7.9	620.0 ±1.0	550 ±10	17 870 ±360	958.0 ±2.0	0.9570 ±0.0020	68 760 ±170	68 750 ±170	1163.0 ±2.0	68 690 ±170	79.2
KC1-8.9	644.0 ±1.0	330 ±10	31 690 ±650	975.0 ±2.0	0.9750 ±0.0020	69 640 ±180	69 630 ±180	1187.0 ±3.0	69 570 ±180	88.5
KC1-9.6	768.0 ±1.0	210 ±4	59 000 ±1230	964.0 ±2.0	0.9770 ±0.0020	70 330 ±220	70 330 ±220	1176.0 ±3.0	70 270 ±220	96.5
KC1-10.1	815.0 ±1.0	1650 ±30	8040 ±160	975.0 ±2.0	0.9860 ±0.0020	70 590 ±180	70 570 ±180	1190.0 ±3.0	70 510 ±180	100.5
KC1-10.6	1011.0 ±1.0	151 ±3	107 570 ±2440	953.0 ±2.0	0.9750 ±0.0020	70 690 ±200	70 690 ±200	1163.0 ±3.0	70 630 ±200	106.0
KC1-11.0	910.0 ±1.0	138 ±3	106 290 ±2420	949.0 ±2.0	0.9750 ±0.0020	70 900 ±200	70 900 ±200	1159.0 ±3.0	70 840 ±200	110.0
KC1-11.3	1166.0 ±2.0	280 ±10	66 270 ±1390	954.0 ±2.0	0.9770 ±0.0020	70 880 ±200	70 880 ±200	1165.0 ±3.0	70 820 ±200	113.0
KC1-11.7	925.0 ±1.0	710 ±10	21 090 ±430	952.0 ±2.0	0.9780 ±0.0010	71 070 ±180	71 060 ±180	1164.0 ±3.0	71 000 ±180	116.6
KC1-12.0	1133.0 ±2.0	143 ±3	128 810 ±2770	955.0 ±2.0	0.9840 ±0.0020	71 470 ±240	71 470 ±240	1169.0 ±3.0	71 410 ±240	120.0
KC1-12.8	1180.0 ±3.0	340 ±10	56 310 ±1270	951.0 ±3.0	0.9850 ±0.0040	71 760 ±390	71 760 ±390	1165.0 ±4.0	71 700 ±390	128.0
KC1-13.1	916.0 ±1.0	710 ±10	21 160 ±430	974.0 ±2.0	0.9960 ±0.0020	71 720 ±210	71 710 ±210	1192.0 ±3.0	71 650 ±210	131.1
KC1-13.6	1148.0 ±1.0	450 ±10	41 300 ±850	954.0 ±2.0	0.9890 ±0.0020	72 010 ±190	72 000 ±190	1169.0 ±3.0	71 940 ±190	136.0
BA1b-0.2	395.1 ±0.4	250 ±10	17 730 ±370	340.0 ±2.0	0.6870 ±0.0010	75 590 ±230	75 580 ±230	421.0 ±2.0	75 520 ±230	2.4
BA1b-1.0	287.0 ±1.0	480 ±10	6960 ±100	369.0 ±3.0	0.7060 ±0.0030	75 960 ±560	75 930 ±560	457.0 ±4.0	75 870 ±560	10.0
BA1b-1.4	445.0 ±1.0	410 ±10	12 680 ±260	360.0 ±2.0	0.7010 ±0.0010	76 010 ±230	75 990 ±230	446.0 ±2.0	75 930 ±230	14.0
BA1b-1.7	457.0 ±1.0	350 ±10	14 840 ±300	357.0 ±2.0	0.6980 ±0.0010	75 810 ±250	75 790 ±250	442.0 ±2.0	75 730 ±250	17.0
BA1b-1.9	416.0 ±1.0	350 ±10	13 570 ±280	358.0 ±2.0	0.7010 ±0.0010	76 200 ±230	76 190 ±230	443.0 ±2.0	76 130 ±230	19.4
BA1b-2.3	338.1 ±0.3	11 910 ±240	310 ±10	282.0 ±2.0	0.6710 ±0.0010	78 210 ±220	77 450 ±580	351.0 ±2.0	77 390 ±580	23.0
BA1b-2.4	496.0 ±1.0	230 ±10	25 460 ±540	357.0 ±2.0	0.7100 ±0.0010	77 690 ±240	77 680 ±240	444.0 ±2.0	77 620 ±240	24.0
BA1b-3.0	613.0 ±1.0	187 ±4	38 250 ±810	348.0 ±2.0	0.7080 ±0.0010	78 170 ±260	78 160 ±260	434.0 ±2.0	78 100 ±260	30.4
BA1b-4.0	659.0 ±1.0	2340 ±50	3350 ±70	367.0 ±2.0	0.7200 ±0.0010	78 370 ±230	78 300 ±240	457.0 ±2.0	78 240 ±240	40.0
BA1b-5.8	691.0 ±1.0	450 ±10	18 080 ±370	362.0 ±2.0	0.7190 ±0.0010	78 650 ±230	78 630 ±230	452.0 ±2.0	78 570 ±230	58.0
BA1b-6.8	490.0 ±1.0	1630 ±30	3570 ±70	355.0 ±2.0	0.7180 ±0.0010	79 120 ±230	79 050 ±230	444.0 ±2.0	78 990 ±230	68.0
BA1b-8.5	519.0 ±1.0	260 ±10	23 460 ±490	359.0 ±2.0	0.7210 ±0.0010	79 180 ±240	79 170 ±240	448.0 ±2.0	79 110 ±240	85.0
BA1b-8.9	523.0 ±1.0	2050 ±30	3010 ±60	345.0 ±2.0	0.7160 ±0.0010	79 640 ±220	79 560 ±220	432.0 ±2.0	79 500 ±220	89.4
BA1b-9.5	516.0 ±1.0	2870 ±60	2150 ±40	358.0 ±2.0	0.7270 ±0.0010	80 170 ±240	80 060 ±260	448.0 ±2.0	80 000 ±260	95.0
BA1b-11.0	507.0 ±1.0	880 ±20	6770 ±140	336.0 ±2.0	0.7140 ±0.0010	80 120 ±270	80 090 ±270	422.0 ±2.0	80 030 ±270	109.8
BA1b-12.0	422.0 ±1.0	310 ±10	16 000 ±390	336.0 ±4.0	0.7120 ±0.0030	79 910 ±620	79 900 ±620	421.0 ±5.0	79 840 ±620	119.8
BA1b-12.9	435.0 ±1.0	20 100 ±400	260 ±10	336.0 ±2.0	0.7190 ±0.0020	80 900 ±290	79 960 ±730	421.0 ±2.0	79 900 ±730	128.8
BA1b-13.7	561.0 ±1.0	1160 ±20	5800 ±120	350.0 ±2.0	0.7260 ±0.0010	80 700 ±260	80 660 ±260	440.0 ±2.0	80 600 ±260	137.0
BA1b-14.5	333.3 ±0.3	17 940 ±360	223 ±4	344.0 ±2.0	0.7280 ±0.0010	81 680 ±250	80 580 ±810	432.0 ±2.0	80 520 ±810	145.0
BA1-0.5	785.0 ±1.0	5270 ±110	1770 ±40	334.0 ±2.0	0.7190 ±0.0010	81 210 ±260	81 070 ±280	419.0 ±2.0	81 010 ±280	5
BA1-0.9	706.0 ±2.0	1860 ±10	4510 ±30	334.0 ±3.0	0.7190 ±0.0030	81 050 ±530	81 000 ±530	420.0 ±3.0	80 940 ±530	10
BA1-3.0	732.0 ±1.0	1060 ±20	8180 ±170	327.0 ±2.0	0.7160 ±0.0010	81 410 ±290	81 380 ±290	411.0 ±2.0	81 320 ±290	30
BA1-5.5	669.0 ±1.0	620 ±10	12 880 ±250	345.0 ±2.0	0.7290 ±0.0030	81 670 ±530	81 660 ±530	435.0 ±3.0	81 600 ±530	56
BA1-9.5	825.0 ±1.0	5170 ±100	1930 ±40	351.0 ±2.0	0.7340 ±0.0010	81 880 ±250	81 750 ±270	443.0 ±2.0	81 690 ±270	95
BA1-10.0	539.0 ±1.0	9480 ±190	690 ±10	351.0 ±2.0	0.7350 ±0.0020	82 160 ±300	81 810 ±390	442.0 ±2.0	81 750 ±390	100
BA1-10.6	829.0 ±1.0	3860 ±80	2610 ±50	351.0 ±2.0	0.7370 ±0.0010	82 530 ±270	82 430 ±270	443.0 ±2.0	82 370 ±270	106
BA1-13.9	643.0 ±1.0	3360 ±70	2300 ±50	332.0 ±2.0	0.7270 ±0.0010	82 700 ±270	82 590 ±280	419.0 ±2.0	82 530 ±280	139
BA1-16.2	459.0 ±1.0	4810 ±20	1140 ±10	325.0 ±2.0	0.7260 ±0.0030	83 160 ±630	82 940 ±630	411.0 ±4.0	82 880 ±630	159
BA1-16.6	454.0 ±1.0	10 280 ±210	520 ±10	308.0 ±2.0	0.7190 ±0.0010	83 600 ±290	83 130 ±440	389.0 ±2.0	83 070 ±440	166
BA1-17.4	443.8 ±0.4	26 460 ±510	202 ±4	303.0 ±1.0	0.7320 ±0.0010	86 420 ±240	85 160 ±920	385.0 ±2.0	85 100 ±920	174
BA1-17.9	573.0 ±1.0	6090 ±120	1130 ±20	305.0 ±2.0	0.7290 ±0.0010	85 640 ±280	85 410 ±320	388.0 ±2.0	85 350 ±320	179
BA1-18.3	545.0 ±1.0	3600 ±70	1810 ±40	304.0 ±2.0	0.7260 ±0.0010	85 220 ±280	85 090 ±290	387.0 ±2.0	85 030 ±290	181
BA1-19.0	381.4 ±0.4	6990 ±140	660 ±10	313.0 ±2.0	0.7350 ±0.0010	85 840 ±260	85 460 ±370	399.0 ±2.0	85 400 ±370	190
BA1-20.8	467.0 ±1.0	2290 ±50	2440 ±50	290.0 ±2.0	0.7260 ±0.0010	86 670 ±290	86 560 ±300	370.0 ±2.0	86 500 ±300	207
BA1-22.0	549.0 ±1.0	22 180 ±440	290 ±10	249.0 ±2.0	0.7120 ±0.0010	88 840 ±280	87 950 ±690	319.0 ±2.0	87 890 ±690	220
BA1-22.5	624.0 ±1.0	2060 ±40	3530 ±70	244.0 ±2.0	0.7080 ±0.0010	88 650 ±290	88 580 ±290	314.0 ±2.0	88 520 ±290	225
BA1-23.6	614.0 ±1.0	3610 ±70	1990 ±40	243.0 ±1.0	0.7080 ±0.0010	88 760 ±270	88 630 ±290	312.0 ±2.0	88 570 ±290	236
BA1-24.2	829.0 ±1.0	3860 ±80	168 ±3	239.0 ±2.0	0.7160 ±0.0010	90 730 ±330	89 160 ±1160	307.0 ±3.0	89 100 ±1160	242
BA1-24.9	319.0 ±1.0	29 560 ±1130	128 ±1	230.0 ±4.0	0.7180 ±0.0060	92 250 ±1300	90 150 ±1650	296.0 ±5.0	90 090 ±1650	246
BA1-25.2	469.0 ±1.0	53 270 ±1070	109 ±2	280.0 ±2.0	0.7510 ±0.0010	92 360 ±420	89 910 ±1790	361.0 ±2.0	89 850 ±1790	252
BA1-25.9	580.0 ±1.0	39 630 ±790	178 ±4	267.0 ±2.0	0.7380 ±0.0010	91 510 ±320	90 020 ±1100	344.0 ±3.0	89 960 ±1100	259
BA1-26.4	746.0 ±1.0	56 260 ±1130	160 ±3	266.0 ±2.0	0.7340 ±0.0010	90 870 ±300	89 230 ±1200	342.0 ±2.0	89 170 ±1200	264
BA2-0.2	635.0 ±1.0	490 ±10	15 060 ±310	240.0 ±2.0	0.7050 ±0.0010	88 590 ±310	88 570 ±310	308.0 ±2.0	88 510 ±310	1.8
BA2-0.5	486.0 ±1.0	7220 ±150	790 ±20	240.0 ±2.0	0.7100 ±0.0010	89 370 ±260	89 040 ±350	309.0 ±2.0	88 980 ±350	4.6
BA2-0.7	655.0 ±1.0	1170 ±20	6530 ±130	240.0 ±2.0	0.7050 ±0.0010	88 590 ±370	88 550 ±370	308.0 ±3.0	88 490 ±370	7
BA2-1.1	474.0 ±1.0	650 ±10	8400 ±170	233.0 ±2.0	0.7040 ±0.0010	89 090 ±290	89 050 ±290	300.0 ±2.0	88 990 ±290	11
BA2-1.6	517.0 ±1.0	1140 ±20	5320 ±110	242.0 ±2.0	0.7090 ±0.0010	89 030 ±330	88 980 ±340	311.0 ±2.0	88 920 ±340	16.0
BA2-2.0	616.0 ±1.0	2390 ±50	3050 ±60	256.0 ±2.0	0.7180 ±0.0010	89 060 ±290	88 970 ±300	329.0 ±2.0	88 910 ±300	20.0
BA2-2.4	904.0 ±1.0	2210 ±40	4880 ±100	260.0 ±2.0	0.7220 ±0.0010	89 300 ±320	89 250 ±320	335.0 ±2.0	89 190 ±320	24.4
BA2-3.0	919.0 ±1.0	6070 ±120	1790 ±40	258.0 ±2.0	0.7190 ±0.0020	89 040 ±340	88 900 ±360	332.0 ±2.0	88 840 ±360	30.0
BA2-3.3	807.0 ±1.0	1580 ±30	6070 ±120	258.0 ±2.0	0.7220 ±0.0010	89 500 ±320	89 450 ±320	333.0 ±2.0	89 390 ±320	33.0
BA2-3.7	372.5 ±0.3	2220 ±40	2000 ±40	258.0 ±2.0	0.7220 ±0.0010	89 490 ±270	89 360 ±280	332.0 ±2.0	89 300 ±280	37.4
BA2-4.5	434.0 ±1.0	7070 ±140	730 ±20	254.0 ±2.0	0.7230 ±0.0010	90 230 ±310	89 880 ±400	328.0 ±2.0	89 820 ±400	45.0
BA2-5.5	408.4 ±0.4	1240 ±30	3910 ±80	258.0 ±2.0	0.7210 ±0.0010	89 480 ±290	89 410 ±290	332.0 ±2.0	89 350 ±290	55.0
BA2-5.9	449.0 ±1.0	700 ±10	7590 ±150	257.0 ±2.0	0.7220 ±0.0010	89 590 ±320	89 560 ±330	331.0 ±2.0	89 500 ±330	58.6
BA2-6.3	444.1 ±0.4	3170 ±60	1670 ±30	259.0 ±2.0	0.7230 ±0.0010	89 550 ±310	89 390 ±330	334.0 ±2.0	89 330 ±330	63.0
BA2-6.9	477.0 ±1.0	970 ±20	5860 ±120	258.0 ±2.0	0.7250 ±0.0010	90 150 ±300	90 100 ±300	333.0 ±2.0	90 040 ±300	69.0
BA2-7.1	528.0 ±1.0	1050 ±20	5940 ±120	253.0 ±2.0	0.7200 ±0.0010	89 730 ±320	89 680 ±320	326.0 ±2.0	89 620 ±320	70.8
BA2-7.8	431.0 ±1.0	3540 ±70	1450 ±30	253.0 ±2.0	0.7210 ±0.0010	89 960 ±330	89 780 ±350	326.0 ±2.0	89 720 ±350	78.0
BA2-8.4	483.0 ±1.0	7840 ±160	730 ±20	247.0 ±2.0	0.7170 ±0.0010	90 050 ±300	89 690 ±390	318.0 ±2.0	89 630 ±390	83.6
BA2-8.5	380.9 ±0.4	2990 ±60	1500 ±30	248.0 ±2.0	0.7160 ±0.0010	89 620 ±280	89 450 ±310	319.0 ±2.0	89 390 ±310	85.0
BA2-9.1	339.6 ±0.3	9230 ±190	440 ±10	265.0 ±2.0	0.7290 ±0.0010	90 030 ±280	89 440 ±500	341.0 ±2.0	89 380 ±500	91.4

Table 1. Continued.

Sample	^{238}U [ppb]	^{232}Th [ppt]	^{230}Th/^{232}Th [atomic x10^{-6}]	δ^{234}U[a] [measured]	^{230}Th/^{238}U [activity]	Age [a] [uncorr.]	Age [a] [corr.]	δ^{234}U$_{Initial}$[b] [corr.]	Age [a BP][c] [corr.]	DFT [mm][d] isotrack-scale
EXC3-0.2	1070.0 ±1.0	240 ±10	51 710 ±1090	148.0 ±2.0	0.7050 ±0.0010	101 000 ±400	101 000 ±400	197.0 ±2.0	100 940 ±400	2.0
EXC3-1.7	1554.0 ±2.0	125 ±3	144 100 ±3300	143.0 ±2.0	0.7020 ±0.0010	101 060 ±350	101 060 ±350	191.0 ±2.0	101 000 ±350	17.0
EXC3-2.9	1709.0 ±3.0	400 ±10	49 380 ±1010	144.0 ±2.0	0.7040 ±0.0010	101 370 ±420	101 360 ±420	192.0 ±2.0	101 300 ±420	29.4
EXC3-4.1	1450.0 ±3.0	87 ±2	193 690 ±4760	146.0 ±2.0	0.7080 ±0.0020	101 900 ±470	101 900 ±470	195.0 ±2.0	101 840 ±470	40.7
EXC3-4.2	1403.0 ±2.0	174 ±4	93 640 ±2040	148.0 ±2.0	0.7060 ±0.0010	101 230 ±390	101 230 ±390	197.0 ±2.0	101 170 ±390	41.4
EXC3-4.3	1071.0 ±1.0	500 ±10	25 090 ±510	149.0 ±1.0	0.7070 ±0.0010	101 250 ±300	101 240 ±300	199.0 ±2.0	101 180 ±300	42.9
EXC3-4.4	1254.0 ±2.0	470 ±10	31 460 ±640	151.0 ±1.0	0.7150 ±0.0010	102 680 ±380	102 670 ±380	202.0 ±2.0	102 610 ±380	44.4
EXC3-4.7	970.0 ±3.0	30 ±10	437 650 ±110310	153.0 ±3.0	0.7170 ±0.0030	102 990 ±850	102 990 ±850	204.0 ±4.0	102 930 ±850	47.4
EXC3-6.8	1415.0 ±2.0	400 ±10	41 590 ±850	150.0 ±1.0	0.7160 ±0.0010	103 160 ±360	103 150 ±360	201.0 ±2.0	103 090 ±360	68.0
EXC3-8.0	1060.0 ±2.0	182 ±4	69 300 ±1480	153.0 ±2.0	0.7200 ±0.0010	103 650 ±410	103 640 ±410	205.0 ±2.0	103 580 ±410	81.9
EXC3-9.0	1259.0 ±1.0	188 ±4	79 020 ±1680	148.0 ±1.0	0.7160 ±0.0010	103 650 ±370	103 640 ±370	198.0 ±2.0	103 580 ±370	90.0
EXC3-11.5	1084.0 ±1.0	102 ±2	126 160 ±2960	150.0 ±2.0	0.7190 ±0.0010	103 890 ±370	103 890 ±370	201.0 ±2.0	103 830 ±370	115.0
EXC3-12.8	976.0 ±1.0	62 ±2	185 870 ±5760	147.0 ±2.0	0.7180 ±0.0010	104 160 ±380	104 160 ±380	197.0 ±2.0	104 100 ±380	127.7
EXC3-14.3	1331.0 ±2.0	158 ±3	99 650 ±2190	145.0 ±1.0	0.7170 ±0.0010	104 340 ±370	104 340 ±370	195.0 ±2.0	104 280 ±370	142.8
EXC3-15.4	1124.0 ±1.0	37 ±1	359 130 ±12980	149.0 ±2.0	0.7200 ±0.0010	104 420 ±370	104 420 ±370	200.0 ±2.0	104 360 ±370	153.9
EXC3-16.1	1393.0 ±2.0	41 ±1	401 510 ±14620	148.0 ±2.0	0.7210 ±0.0010	104 620 ±390	104 620 ±390	199.0 ±2.0	104 560 ±390	161.4
EXC3-17.1	1266.0 ±2.0	550 ±10	27 210 ±550	144.0 ±2.0	0.7190 ±0.0010	104 860 ±430	104 850 ±430	193.0 ±2.0	104 790 ±430	170.9
EXC3-17.9	1533.0 ±2.0	520 ±10	34 820 ±710	139.0 ±2.0	0.7180 ±0.0010	105 660 ±440	105 650 ±440	187.0 ±2.0	105 590 ±440	179.0
EXC3-18.7	1176.0 ±2.0	1000 ±20	14 040 ±280	141.0 ±2.0	0.7210 ±0.0020	105 890 ±480	105 870 ±480	190.0 ±2.0	105 810 ±480	187.8
EXC3-20.0	123.1 ±0.1	132 ±3	11 140 ±220	141.0 ±2.0	0.7220 ±0.0010	106 070 ±380	106 040 ±380	190.0 ±2.0	105 980 ±380	200.0
EXC3-20.9	1372.0 ±2.0	430 ±10	37 540 ±763	139.0 ±1.0	0.7200 ±0.0010	105 950 ±370	105 940 ±370	188.0 ±2.0	105 880 ±370	208.7
EXC3-21.8	1254.0 ±1.0	183 ±4	81 860 ±1730	145.0 ±2.0	0.7260 ±0.0010	106 270 ±410	106 270 ±410	196.0 ±2.0	106 210 ±410	217.7
EXC3-22.6	1393.0 ±2.0	990 ±20	16 880 ±340	147.0 ±2.0	0.7290 ±0.0010	106 830 ±410	106 810 ±410	198.0 ±2.0	106 750 ±410	225.9
EXC3-23.4	2979.0 ±5.0	790 ±20	5580 ±930	147.0 ±2.0	0.7300 ±0.0020	106 920 ±460	106 910 ±460	199.0 ±2.0	106 850 ±460	233.9
EXC3-24.3	1061.0 ±2.0	250 ±10	51 260 ±1070	145.0 ±2.0	0.7300 ±0.0010	107 520 ±420	107 520 ±420	196.0 ±2.0	107 460 ±420	243.0
EXC3-24.6	895.0 ±2.0	70 ±10	144 720 ±13520	145.0 ±3.0	0.7330 ±0.0030	108 050 ±880	108 050 ±880	197.0 ±3.0	107 990 ±880	246.2
EXC3-25.5	1233.0 ±2.0	92 ±2	160 930 ±4020	141.0 ±2.0	0.7310 ±0.0010	108 170 ±410	108 170 ±410	192.0 ±2.0	108 110 ±410	254.7
EXC3-26.0	1009.0 ±2.0	370 ±10	32 830 ±670	146.0 ±2.0	0.7340 ±0.0020	108 170 ±490	108 160 ±490	198.0 ±2.0	108 100 ±490	260.0
EXC3-26.8	1076.0 ±1.0	830 ±20	15 800 ±320	147.0 ±2.0	0.7350 ±0.0010	108 290 ±400	108 270 ±400	200.0 ±2.0	108 210 ±400	267.9
EXC3-27.8	941.0 ±2.0	73 ±2	155 730 ±3850	146.0 ±2.0	0.7380 ±0.0020	109 030 ±500	109 030 ±500	199.0 ±2.0	108 970 ±500	278.0
EXC3-28.9	763.0 ±2.0	1050 ±10	8850 ±90	144.0 ±2.0	0.7400 ±0.0030	109 950 ±920	109 910 ±920	197.0 ±3.0	109 850 ±920	290.4
EXC3-29.5	872.0 ±1.0	124 ±3	86 130 ±1980	144.0 ±1.0	0.7400 ±0.0010	110 060 ±400	110 060 ±400	197.0 ±2.0	110 000 ±400	294.9
EXC4-12.4	877.0 ±1.0	115 ±3	76 440 ±1830	174.0 ±2.0	0.6060 ±0.0010	77 510 ±230	77 510 ±230	216.0 ±2.0	77 450 ±230	122.3
EXC4-15.2	1213.0 ±2.0	470 ±10	25 730 ±520	171.0 ±2.0	0.6090 ±0.0010	78 290 ±250	78 280 ±250	214.0 ±2.0	78 220 ±250	152.3
EXC4-18.0	830.0 ±1.0	2500 ±50	3350 ±70	177.0 ±2.0	0.6130 ±0.0010	78 460 ±300	78 390 ±310	221.0 ±2.0	78 330 ±310	183.5
EXC4-21.4	793.0 ±1.0	100 ±2	82 720 ±2000	162.0 ±2.0	0.6170 ±0.0010	80 770 ±270	80 770 ±270	204.0 ±2.0	80 710 ±270	218.8
EXC4-24.1	694.0 ±2.0	260 ±10	27 210 ±680	162.0 ±3.0	0.6260 ±0.0030	82 530 ±660	82 520 ±660	205.0 ±4.0	82 460 ±660	244.8
EXC4-25.1	832.0 ±1.0	740 ±20	11 560 ±230	160.0 ±1.0	0.6270 ±0.0010	82 900 ±270	82 880 ±270	202.0 ±2.0	82 820 ±270	250.8
EXC4-25.5	771.0 ±1.0	115 ±3	74 850 ±1710	143.0 ±2.0	0.6750 ±0.0010	94 880 ±370	94 880 ±370	187.0 ±2.0	94 820 ±370	255.3
EXC4-26.8	1008.0 ±1.0	640 ±10	17 640 ±360	142.0 ±2.0	0.6780 ±0.0010	95 820 ±320	95 810 ±320	186.0 ±2.0	95 750 ±320	267.3
EXC4-29.1	782.0 ±1.0	22 ±1	401 480 ±23250	140.0 ±2.0	0.6840 ±0.0010	97 530 ±390	97 530 ±390	184.0 ±2.0	97 470 ±390	291.8
EXC4-30.5	830.0 ±1.0	400 ±10	23 810 ±490	140.0 ±2.0	0.6920 ±0.0010	99 320 ±340	99 310 ±340	185.0 ±2.0	99 250 ±340	305.0
EXC4-32.0	1025.0 ±1.0	142 ±3	82 600 ±1900	131.0 ±1.0	0.6940 ±0.0010	101 220 ±360	101 210 ±360	174.0 ±2.0	101 150 ±360	319.8
EXC4-33.0	958.0 ±1.0	160 ±3	69 050 ±1490	134.0 ±2.0	0.7000 ±0.0010	102 020 ±380	102 020 ±380	179.0 ±2.0	101 960 ±380	330.0
EXC4-33.1	853.0 ±2.0	16 ±10	608 880 ±264500	141.0 ±2.0	0.7070 ±0.0030	102 510 ±790	102 510 ±790	189.0 ±3.0	102 450 ±790	334.8
EXC4-34.1	794.0 ±1.0	250 ±10	38 060 ±790	143.0 ±2.0	0.7140 ±0.0010	103 780 ±410	103 770 ±410	192.0 ±2.0	103 710 ±410	344.0
EXC4-35.5	787.0 ±1.0	320 ±10	29 010 ±590	141.0 ±1.0	0.7150 ±0.0010	104 530 ±360	104 520 ±360	189.0 ±2.0	104 460 ±360	355.3
EXC4-36.0	965.0 ±1.0	1420 ±30	8050 ±160	142.0 ±2.0	0.7190 ±0.0010	105 260 ±350	105 220 ±350	191.0 ±2.0	105 160 ±350	360.0
EXC4-37.0	942.0 ±1.0	540 ±10	20 850 ±420	142.0 ±1.0	0.7210 ±0.0010	105 730 ±360	105 710 ±360	191.0 ±2.0	105 650 ±360	369.8
EXC4-37.5	911.0 ±2.0	210 ±10	51 130 ±1610	146.0 ±2.0	0.7280 ±0.0030	106 740 ±820	106 730 ±820	198.0 ±3.0	106 670 ±820	378.5
EXC4-38.4	896.0 ±1.0	2350 ±50	4600 ±90	147.0 ±2.0	0.7300 ±0.0010	107 200 ±370	107 140 ±380	198.0 ±2.0	107 080 ±380	383.8
SCH7-0.6	113.0 ±0.1	920 ±20	1700 ±30	266.0 ±2.0	0.8380 ±0.0020	112 190 ±540	112 020 ±550	365.0 ±3.0	111 960 ±550	5.5
SCH7-1.2	130.1 ±0.1	1820 ±40	990 ±20	262.0 ±2.0	0.8390 ±0.0020	112 950 ±470	112 650 ±510	360.0 ±3.0	112 590 ±510	12.0
SCH7-2.4	110.3 ±0.1	2250 ±50	680 ±10	252.0 ±2.0	0.8370 ±0.0020	114 230 ±480	113 790 ±570	348.0 ±3.0	113 730 ±570	24.0
SCH7-2.6	113.4 ±0.1	3040 ±60	510 ±10	248.0 ±2.0	0.8310 ±0.0020	113 720 ±500	113 130 ±650	341.0 ±3.0	113 070 ±650	26.3
SCH7-3.0	133.5 ±0.1	5250 ±110	350 ±10	252.0 ±2.0	0.8400 ±0.0020	114 980 ±520	114 120 ±790	348.0 ±3.0	114 060 ±790	30.0
SCH7-3.5	118.7 ±0.1	340 ±10	4850 ±100	261.0 ±2.0	0.8470 ±0.0020	114 950 ±530	114 890 ±530	361.0 ±3.0	114 830 ±530	34.5
SCH7-4.5	119.6 ±0.1	59 ±2	28 310 ±900	268.0 ±2.0	0.8540 ±0.0020	115 420 ±530	115 410 ±530	371.0 ±2.0	115 350 ±530	45.0
SCH7-5.5	156.7 ±0.2	94 ±2	23 430 ±550	266.0 ±2.0	0.8520 ±0.0020	115 210 ±470	115 200 ±470	368.0 ±3.0	115 140 ±470	54.8
SCH7-5.9	111.2 ±0.1	67 ±2	23 260 ±590	263.0 ±2.0	0.8520 ±0.0020	115 750 ±510	115 730 ±510	365.0 ±3.0	115 670 ±510	59.0
SCH7-6.1	138.0 ±0.1	220 ±10	9000 ±200	267.0 ±2.0	0.8520 ±0.0020	115 020 ±510	114 990 ±510	369.0 ±3.0	114 930 ±510	61.0
SCH7-6.5	157.4 ±0.2	116 ±3	19 160 ±420	266.0 ±2.0	0.8530 ±0.0020	115 460 ±470	115 450 ±470	369.0 ±3.0	115 390 ±470	65.0
SCH7-7.0	139.0 ±0.1	370 ±10	5330 ±110	268.0 ±2.0	0.8530 ±0.0020	115 090 ±450	115 030 ±450	371.0 ±2.0	114 970 ±450	70.0
SCH7-7.4	165.2 ±0.2	181 ±4	12 960 ±270	273.0 ±2.0	0.8620 ±0.0020	116 530 ±490	116 500 ±490	379.0 ±3.0	116 440 ±490	74.0
SCH7-8.0	136.3 ±0.1	230 ±10	8400 ±180	265.0 ±2.0	0.8540 ±0.0020	115 910 ±500	115 870 ±500	368.0 ±2.0	115 810 ±500	80.3
SCH7-9.0	160.5 ±0.2	790 ±20	2890 ±60	264.0 ±2.0	0.8580 ±0.0020	116 900 ±500	116 790 ±510	368.0 ±3.0	116 730 ±510	90.0
SCH7-9.7	165.7 ±0.1	320 ±10	7220 ±150	260.0 ±2.0	0.8570 ±0.0010	117 470 ±440	117 430 ±440	363.0 ±2.0	117 370 ±440	96.8
SCH7-10.3	201.0 ±0.2	850 ±20	3340 ±70	260.0 ±2.0	0.8570 ±0.0020	117 500 ±480	117 410 ±480	362.0 ±3.0	117 350 ±480	102.8
SCH7-11.0	139.6 ±0.1	143 ±3	13 650 ±300	248.0 ±2.0	0.8490 ±0.0020	117 720 ±500	117 700 ±500	346.0 ±2.0	117 640 ±500	110.0
SCH7-11.3	147.5 ±0.2	143 ±3	14 330 ±320	239.0 ±2.0	0.8430 ±0.0020	118 000 ±550	117 980 ±550	334.0 ±3.0	117 920 ±550	113.3
SCH7-11.4	117.2 ±0.1	1350 ±30	1220 ±30	242.0 ±2.0	0.8500 ±0.0020	119 060 ±490	118 810 ±520	339.0 ±2.0	118 750 ±520	114.0

[a] δ^{234}U $= ([^{234}$U$/^{238}$U$]_{activity} - 1) \times 1000$. δ^{234}U$_{initial}$ was calculated based on ^{230}Th age (T), i.e., δ^{234}U$_{initial} = \delta^{234}U_{measured} \times e^{\lambda 234 x T}$. [b] Corrected ^{230}Th ages assume the initial ^{230}Th/^{232}Th atomic ratio of $4.4 \pm 2.2 \times 10^{-6}$. Those are the values for a material at secular equilibrium, with the bulk earth ^{232}Th/^{238}U value of 3.8. The errors are arbitrarily assumed to be 50 %. [c] a BP stands for "years Before Present" where the present is defined as the year 1950 A.D. [d] DFT stands for "Distance From Top" of the stalagmite.
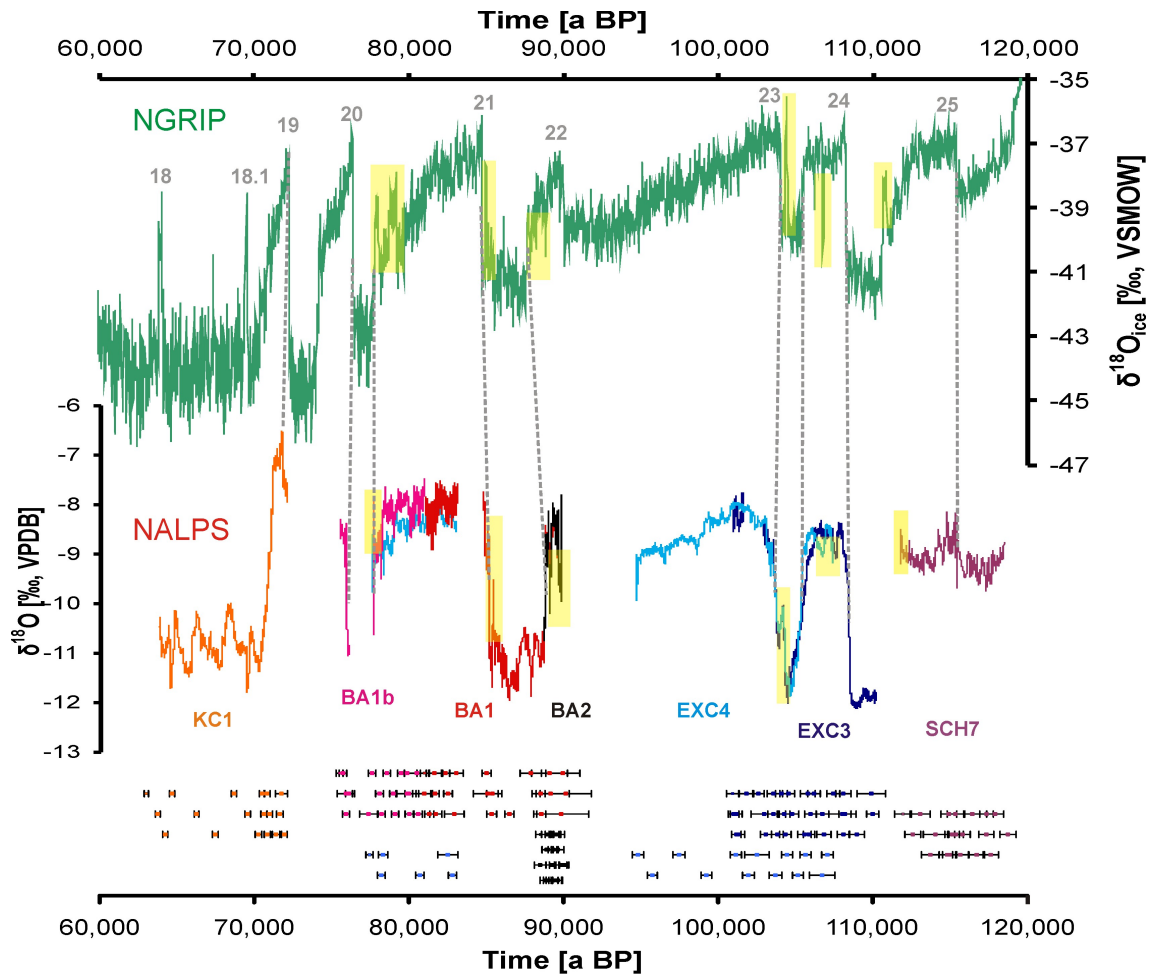
Fig. 2. The NALPS record (consisting of seven stalagmites) compared to NGRIP plotted on the GICC05modelext timescale in the interval from 120 to 60 ka. Individual U-Th ages and associated 2σ-uncertainties are plotted at the bottom. The grey, dashed lines connect the mid-points of major D-O transitions or isotopic maxima. The recurrent warm Greenland Interstadials of the D-O cycles are indicated by grey numbers. Short-lived warming and cooling events (sub-D-O events) are highlighted by the yellow rectangles. NALPS confirms the Greenland chronology for the early part of the Last Glacial period, but suggests younger ages of rapid stadial and interstadial transitions between ca. 106 and 60 ka, and a longer duration of the stadial following GI 22.

reflect the O isotopic composition of regional meteoric precipitation and in the Alps this variable is strongly correlated with air temperature (Rozanski et al., 1992; Humer et al., 1995; Kaiser et al., 2001). Moreover, the temperature of carbonate precipitation in the cave is directly related to the outside air temperature and determines the O isotopic fractionation between drip water and speleothem calcite (Friedman and O'Neil, 1977; Kim and O'Neil, 1997; Lachniet, 2009). Therefore, the air temperature has a major, combined effect on the speleothem O isotopic composition. Seasonality, however, might also affect the isotope signal in the Alps (Humer et al., 1995), as the seasonal amplitude in $\delta^{18}O$ of meteoric precipitation is around 10 ‰ (IAEA/WMO, 2010). The distribution of precipitation during the warm and cold season might thus exert a major influence on the overall isotopic composition. This could partially explain the large shifts at

the D-O transitions. Major changes in the source region of precipitation, e.g. Atlantic vs. Mediterranean (cf. Spötl et al., 2010), are considered negligible on the northern rim of the Alps, whereas changes in the trajectories of moisture across the European continent might have some influence (cf. Sodemann and Zubler, 2010). Replication of intervals in different stalagmite samples suggests neither cave-specific nor drip site-specific effects had a major influence on the O isotopic composition. The unsaturated zone above the studied caves ranges from ca. 10 to 200 m allowing for fast transmission of the meteoric O isotopic signal by the seepage water.

A synchronous occurrence of the rapid climate changes recorded in Greenland and NALPS is a reasonable assumption given the location of the selected cave sites at the northern, Atlantic-exposed rim of the Alps. The records reveal eye-catching similarities in the detailed pattern of individual

D-O events between the Alps and Greenland. Most of the events are very similar in the duration and relative amplitudes at both locations. Moreover, the details recorded both in the ice and stalagmite isotope curves, e.g. the short-lived sub-D-O warming and cooling events (see Sect. 6), are a strong argument for synchronicity between Greenland and Europe. An asynchronous or systematically different climate evolution in the two regions is clearly not supported by the data and we therefore do not discuss potential leads and lags or systematic offsets. The observed differences in the timing of the D-O events most likely originate from the different chronologies, i.e. a problem that can be solved within the dating uncertainties of the Greenland and NALPS records. For that reason we concentrate on discussing these chronological issues.

In general, the rapid transitions of 1 to 4.5 ‰ in δ^{18}O took place within decades (central shift) to several centuries (whole transition) in our samples (Table 2). The central shift encompasses the abrupt and also largest part of the amplitude of a D-O transition. The whole transition also includes the less abrupt, i.e. more gradual flanks and the entire amplitude of a transition. In particular, the transition from Marine Isotope Stage (MIS) 5 to 4, i.e. the D-O 19 cooling, lasted 400 yr in its central portion (2.8 ‰ shift) and 950 yr for the whole transition (4.3 ‰; Fig. 3; stalagmite KC1). The D-O 20 warming lasted 110 yr (2.6 ‰, stalagmite BA1b) and D-O 21 cooling 20 yr (2.7 ‰, BA1b; the event, however, is not recorded completely). The central portion of the D-O 21 rapid warming (2.3 ‰; BA1) lasted 60 yr, while the whole transition took place within 550 yr (4.0 ‰, BA1). The cooling of D-O 22 occurred within 60 yr (2.2 ‰; stalagmite BA2) and the cooling of D-O 24 lasted 120 yr in its central part (1.2 ‰) and 1050 yr for the whole transition (3.3 ‰, EXC4). Stalagmite EXC3 recorded the warmings of D-O 23 and 24: the central shifts of 2.2 ‰ each occurred within 340 and 170 yr, respectively, while the whole transitions of 3.6 and 3.5 ‰ lasted 1400 and 590 yr, respectively. The minor D-O 25 warming (1.5 ‰) lasted 20 yr in our record (Fig. 3; stalagmite SCH7).

5 Chronological implications

Significant chronological implications arise for the current Greenland ice-core timescale. In the following discussion we exclusively use the updated timescale for the NGRIP ice core (GICC05modelext; Wolff et al., 2010). The MIS 5/4 transition, i.e. the D-O 19 cooling transition, is recorded in stalagmite KC1 in great detail (Fig. 2). D-O 19 started with a rapid increase towards positive O isotope values, followed by a gradual cooling over several centuries and a rapid drop towards negative values into MIS 4, which reflects the typical pattern associated with D-O fluctuations (e.g. Rahmstorf, 2002; Peavoy and Franzke, 2010). The GI 19 isotopic maximum occurred at 71 690 ± 220 a BP (average 2σ-error at the isotope maximum), compared to 72 090 a BP in the NGRIP record (Fig. 2). The two tie points (isotopic maxima) thus exhibit a difference of 400 yr, i.e. NALPS suggests a younger age (Fig. 2 and Table 2). In the East Asian cave records (e.g. Wang et al., 2001, 2008) the MIS5/4 transition is not as pronounced as in the NALPS record. D-O transitions in the monsoonal records are generally more gradual and the cold/dry stadials are smoother than in alpine samples. Going further back in time, the rapid transition into GI 20 is constrained to 75 860 ± 300 a (mid-point of the transition; Fig. 2) compared to 76 410 a in the ice-core record, i.e. NALPS is younger by 550 yr. The mid-point of the transition from GI 21 to the subsequent stadial is located at 77 580 ± 240 a in NALPS and at 77 795 a in NGRIP, i.e. a difference of 215 yr.

Regarding the long stadial following GI 22, there is a mismatch between the ice core and the speleothem record (Fig. 2). The transition into GI 21 (mid-point) is constrained to 84 730 a in NGRIP and to 85 030 ± 410 a in stalagmite BA1, i.e. NALPS is only 300 yr older, which is within the error of the associated U-Th ages. The transition from GI 22 into the stadial, however, reveals an age of 87 630 a in NGRIP versus 88 690 ± 330 a in NALPS, i.e. this is the only transition in the first half of the Last Glacial, where NALPS suggests a significantly older age than Greenland (by 1060 yr). The sharp transition into the stadial following GI 22 is recorded in the two stalagmites BA2 and BA1, but is only constrained precisely in BA2 (Fig. 2). For that reason, the age model of BA1 in the overlapping section was adjusted to the age model of BA2 using the software Analy-Series (Paillard et al., 1996). Based on several precise U-Th ages, however, there is a distinct discrepancy in the duration of the stadial: it was approximately 2900 yr long based on the current ice core chronology, while it lasted ca. 3650 yr according to the NALPS record. A relatively long stadial following GI 22 is also supported by East Asian stalagmite records (e.g. Sanbao Cave; Wang et al., 2008).

The D-O transition from into GI 23 is constrained to 103 995 a in NGRIP compared to 103 550 ± 375 a in NALPS, i.e. the latter is 445 yr younger (Fig. 2). The rapid cooling from GI 24 to the subsequent stadial occurred at 105 410 a in the ice core and at 105 210 ± 450 a in stalagmite EXC4, i.e. a difference of 200 yr. The latter transition is also recorded in stalagmite EXC3, although the isotope drop is less pronounced there. A stalagmite record from Corchia Cave, Italy (Drysdale et al., 2007) also covers the time interval from 118 to 96 ka. In this record, the stadial following GI 24 appears rather long and the transition into GI 23 occurs somewhat late compared to NALPS, although it is within the 2σ-age uncertainty (0.8–1.0 kyr; Drysdale et al., 2007). The progression of GI 23 is very similar in both speleothem records, i.e. showing a long-term cooling trend. The mid-point of the transition into GI 24 is constrained to 108 250 a in NGRIP and to 108 300 ± 450 a in NALPS; the small discrepancy of 50 yr is well within the errors of the U-Th age model. Similarly, the transition into GI 25 is constrained to 115 350 a

Table 2. Overview on timing, duration and amplitude of D-O transitions and short-lived sub-D-O events.

Event[a]	Timing[b] [a BP]				Duration of transition[c] [yr]		Amplitude[d] [‰]	
	NALPS	Error, 2σ [a]	NGRIP	Difference [yr]	Central	Whole	Central	Whole
D-O 19 cooling, MIS5/4					400	950	2.8	4.3
D-O 19 isotopic max.	71 690	±220	72 090	−400				
D-O 20 warming	75 860	±300	76 410	−550		110		2.6
D-O 21 cooling	77 580	±240	77 795	−215		20		2.7
D-O 21 warming	85 030	±410	84 730	+300	60	550	2.3	4.0
D-O 22 cooling	88 690	±330	87 630	+1060		60		2.2
D-O 23 warming	103 550	±375	103 995	−445	340	1400	2.2	3.6
D-O 24 cooling	105 210	±450	105 410	−200	120	1050	1.2	3.3
D-O 24 warming	108 300	±450	108 250	+50	170	590	2.2	3.5
D-O 25 warming	115 320	±500	115 350	−30		20		1.5

	From [a BP]	To [a BP]	Duration of event [yr]	Increase/Decrease[e] [‰]
GI 21 rebound	77 730	77 580	150	1.2
GI 21 precursor I	85 440	85 250	190	1.7/−2.2
GI 21 precursor II	85 070	84 970	100	2.4/−1.0
GI 22 transient cooling I	89 700	89 490	210	−1.8
GI 22 transient cooling II	89 130	88 880	250	−2.1
GI 23 precursor	104 170	103 770	400	1.2/−0.8
GI 24 transient cooling	107 620	107 240	380	−0.7
GI 25 rebound	111 780	111 600	180	0.7

[a] D-O events and short-lived sub-D-O warming (precursor and rebound) and cooling events.

[b] Mid-point of the respective transitions in the NALPS and NGRIP (GICC05modelext) records.

[c] Sharp rapid shift (central) is often flanked by more gradual progressions (whole transition) towards isotopic maxima/minima.

[d] Oxygen isotopic amplitude of the central and whole portion of a transition.

[e] Oxygen isotopic increase (positive values) and decrease (negative values) during a particular sub-D-O event.

and $115\,320 \pm 500$ a in NGRIP and NALPS, respectively, i.e. identical within the current dating uncertainties. Compared to NALPS, the stalagmite record from Corchia Cave shows a more gradual and relatively early transition into GI 24 and also a more gradual shift into GI 25. The latter, however, is better developed in the Italian record. In Sanbao Cave (Wang et al., 2008) the maximum of GI 25 occurred relatively late and the transition is much more gradual.

Taken together, the NALPS record suggests overall younger ages for the rapid stadial and interstadial transitions compared to the current NGRIP timescale (GICC05modelext) between 120 and 60 ka (Table 2). This observation is consistent with East Asian stalagmite records (Xia et al., 2007), as well as with the layer-counted GICC05 ice-core timescale for the period younger than 60 ka (Svensson et al., 2008). Moreover, stalagmites from Kleegruben Cave in the Alps also suggest a shift towards younger ages in the ss09sea timescale (Johnsen et al., 2001) in the interval of GI 15 to 14 (Spötl et al., 2006). Based on our U-Th data and age models, the shift towards younger ages is ca. 200–600 yr in the interval 106 to 60 ka, while our data support the current Greenland ice-core timescale between 118 and

106 ka. Notably, the timing of the rapid transitions into and out of the stadial following GI 22 (Fig. 2; Table 2) is older in NALPS than in NGRIP.

6 Details recorded in NALPS

A comparison of the Greenland ice-core records with NALPS reveals a great deal of agreement but also some significant differences. Next to the difference in the duration of the stadial following GI 22 in NGRIP and NALPS (see above), the short-lived D-O events 18 and 18.1 are not recorded in the O isotopic composition of the speleothem record (Fig. 2), although stalagmite KC1 is obviously sensitive to rapid climate changes (it recorded D-O 19) and the mean temporal resolution in the corresponding stalagmite section is high (11 a). In the NGRIP record the maximum amplitude of 4.5 ‰ of D-O 18 is located at 64 010 a and the interstadial lasted from 64 170 to 63 810 a (360 yr). The maximum amplitude of 5.2 ‰ of D-O 18.1 is located at 69 510 a and this warm episode lasted 460 yr (69 630–69 170 a). Interestingly, there is also a lack of clear evidence for D-O 18
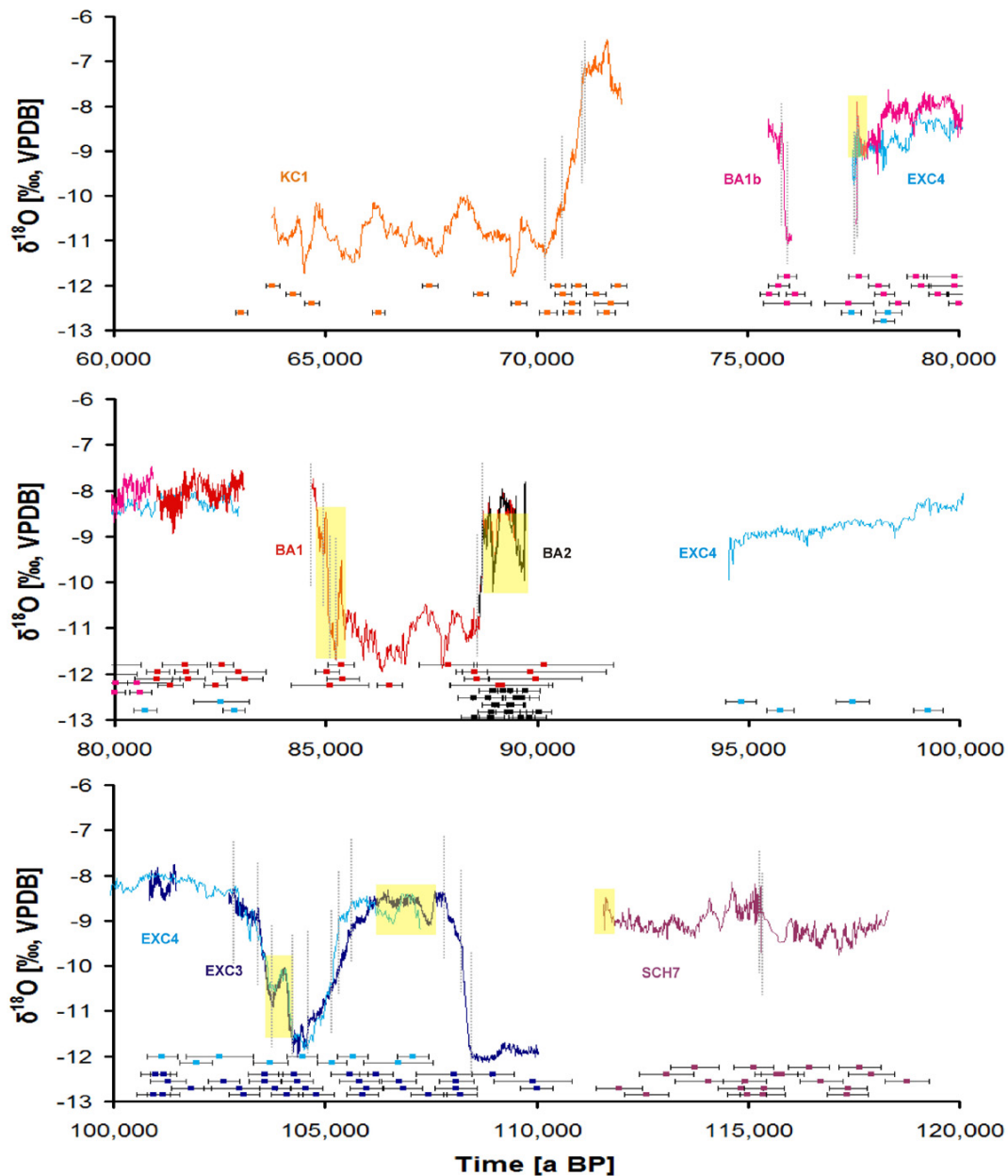
Fig. 3. Detailed structure of the NALPS record. The timing of central and whole D-O transitions (see text) is indicated by the grey, dotted lines. U-Th age data with 2σ-error bars are plotted at the bottom of the diagrams and the yellow rectangles highlight sub-D-O warming and cooling events.

in the East Asian monsoon records from Hulu and Sanbao Cave, although the temporal resolution is high enough to resolve the short interstadial during MIS 4 (Wang et al., 2001; Xia et al., 2007; Wang et al., 2008). With regard to D-O 18.1 there is evidence from new data of Hulu Cave (R. L. Edwards, unpubl. data). The observations in the Alps and East Asia provoke questions regarding the nature of some of these short-lived D-O interstadials, in particular with respect to their regional impact.

The NALPS record further resolves other short-lived details also found in the Greenland ice-core records (Fig. 3, Table 2), i.e. recurrent sub-millennial climate changes within the well-known D-O stadial and interstadial successions recently discussed by Capron et al. (2010). The intermittent climate swings consist of short and abrupt warming events preceding GI 21 and 23 (termed precursor-type events) and of rapid warming events at the end of GI 21 and 25 (termed rebound-type events). Moreover, distinct transient cooling

events are observed during GI 22 and 24. Such superimposed and rapid Last Glacial events have not been documented outside Greenland. In the NGRIP record, a precursor-type climate event preceded GI 21 (Fig. 3, Table 2) and shows a 2.2 ‰ variation in δ^{18}O of ice within 200 yr (Capron et al., 2010). The actual onset of GI 21 coincided with a 4.2 ‰ increase in δ^{18}O of ice, following a 100 yr-return to cold conditions. NALPS provides evidence of two short-lived events preceding GI 21: the first one is centred at 85 360 a and lasted for 190 yr (85 440–85 250 a). It is characterized by a rapid increase of 1.7 ‰ and a subsequent rapid decrease of 2.2 ‰ (Fig. 3). The maximum of the second event is centred at 84 990 a and its duration was 100 yr (85 070–84 970 a). This event consists of a rapid 2.4 ‰ increase followed by a rapid 1.0 ‰ decrease and the final transition into GI 21. At the end of the gradual cooling interval of GI 21 the Greenland O isotope values increased by ca. 2 ‰ in less than 100 yr, before they returned to stadial conditions (Capron et al., 2010). In the NGRIP record this rebound-type event shows two major positive peaks centred at 78 970 and 77 990 a (Fig. 2). The latter, shorter event at the end of GI 21 is also recorded in NALPS: the δ^{18}O maximum occurred at 77 590 a and this distinct rebound of 1.2 ‰ lasted for 150 yr (77 730–77 580 a), followed by a rapid transition into the stadial. Capron et al. (2010) noted that this rebound pattern is similar to GI 22 with regard to its δ^{18}O magnitude, duration and structure. In spite of this, however, it is not counted as a GI. GI 22 is characterized by two distinct cooling events centred at 88 950 and 89 610 a in NALPS (recorded in stalagmite BA2). The O isotope values show decreases of 2.1 and 1.8 ‰ and the anomalies lasted for 250 yr (89 130–88 880 a) and 210 yr (89 700–89 490 a), respectively. The younger of the two events is also recorded in stalagmite BA1, although the associated U-Th age errors are significantly larger. There is also evidence for these cooling anomalies during GI 22 in the NGRIP record (Fig. 2).

Another precursor-type structure is evident immediately prior to GI 23 in Greenland: δ^{18}O increased by 3.8 ‰ within 130 yr and subsequently dropped by 3.6 ‰ in 100 yr. The latter transition back to stadial conditions lasted for 300 yr before the δ^{18}O values increased again by 3 ‰ at the onset of GI 23 (cf. Capron et al., 2010). In the NALPS record this precursor event is centred at 104 050 a (Fig. 3) and is characterized by a positive shift of 1.2 ‰ followed by a negative shift of 0.8 ‰ in δ^{18}O and lasted for about 400 yr (104 170–103 770 a). Going further back in the Last Glacial period, GI 24 shows two distinct negative (cooling) peaks of 100 to 200 yr duration in NGRIP. Based on the GICC05modelext timescale the two minima occurred at 106 770 a and 106 230 a, respectively. NALPS shows the first, more pronounced minimum in two stalagmites and the event is constrained to 107 470 a based on the age model of stalagmite EXC3 (higher resolution and better chronology in this section than sample EXC4). The negative O isotope anomaly of 0.7 ‰ magnitude lasted for 380 yr (107 620–

107 240 a) and its progression is characterized by a rapid decrease and more gradual increase in both stalagmites. Capron et al. (2010) reported that no other interstadial was interrupted by comparable, short, cold events. In the NALPS record, however, two stalagmites document a distinct negative peak during GI 22 (see above). In this context the question whether GI 22 should be considered an interstadial or (only) a rebound-type structure following the long GI 23 (cf. Capron et al., 2010) can be raised again. At the end of GI 25 there is evidence of a rebound-type event in the NALPS record comparable to NGRIP (cf. Capron et al., 2010). The event lasted for ca. 180 yr (111 780–111 600 a) and the maximum positive shift of 0.7 ‰ occurred at 111 660 a based on NALPS (Fig. 3).

Regarding the secondary, sub-millennial events a relationship with the summer insolation at 65° N in connection with variable ice-sheet extensions was discussed (Capron et al., 2010). The rebound-type events are typically associated with relatively low summer insolation at the end of particularly long cooling phases during the GI progression. In contrast, the precursor-type events might be linked to insolation maxima; Capron et al. (2010) reported an in-phase relationship of the GI 21 precursor event with a relative maximum in 65° N summer insolation and a delay of ca. 2.5 kyr of the GI 23 precursor relative to the preceding insolation maximum (after Laskar et al., 2004). Based on the NALPS chronology the precursor of GI 23 (maximum at 104 050 a; cf. Fig. S2 in the Supplement) is delayed by ca. 1 kyr when compared to the adjacent insolation maximum calculated by Laskar et al. (2004). The two precursor events of GI 21 recorded in NALPS (at 85 360 and 84 990 a; Fig. 3) preceded the insolation maximum by ca. 1 to 1.5 kyr (Fig. S2). Using the NALPS chronology in relation to the summer insolation after Laskar et al. (2004) therefore suggests a shorter delay (ca. 1 kyr) of the GI 23 precursor event as compared to Capron et al. (2010). Our data support a preferential occurrence of the precursor events at times of maximum Northern Hemisphere summer insolation during the Last Glacial.

References

Ahn, J. and Brook, E. J.: Atmospheric CO_2 and climate on millennial time scales during the last glacial period, Science, 322, 83–85, 2008.

Alley, R. B., Anandakrishnan, S., and Jung, P.: Stochastic resonance in the North Atlantic, Paleoceanography, 16, 190–198, 2001.

Arz, H. W., Lamy, F., Ganopolski, A., Nowaczyk, N., and Pätzold, J.: Dominant Northern Hemisphere climate control over millennial-scale glacial sea-level variability, Quaternary Sci. Rev., 26, 312–321, 2007.

Asmerom, Y., Polyak, V. J., and Burns, S. J.: Variable winter moisture in the southwestern United States linked to rapid glacial climate shifts, Nat. Geosci., 3, 114–117, 2010.

Auer, I., Böhm, R., Jurkovic, A., Lipa, W., Orlik, A., Potzmann, R., Schöner, W., Ungersböck, M., Matulla, C., Briffa, K., Jones, P., Efthymiadis, D., Brunetti, M., Nanni, T., Maugeri, M., Mercalli, L., Mestre, O., Moisselin, J.-M., Begert, M., Müller-Westermeier, G., Kveton, V., Bochnicek, O., Stastny, P., Lapin, M., Szalai, S., Szentimrey, T., Cegnar, T., Dolinar, M., Gajic-Capka, M., Zaninovic, K., Majstorovic, Z., and Nieplova, E.: HISTALP-historical instrumental climatological surface time series of the Greater Alpine Region, Int. J. Climatol., 27, 17–46, 2007.

Birchfield, G. E., Wang, H., and Rich, J. J.: Century/millennium internal climate variability: an ocean-atmosphere-continental ice sheet model, J. Geophys. Res., 99, 12459–12470, 1994.

Bond, G., Showers, W., Cheseby, M., Lotti, R., Almasi, P., deMenocal, P., Priore, P., Cullen, H., Hajdas, I., and Bonani, G.: A pervasive millennial-scale cycle in North Atlantic Holocene and Glacial climates, Science, 278, 1257–1266, 1997.

Braun, H., Christi, M., Rahmstorf, S., Ganopolski, A., Mangini, A., Kubatski, C., Roth, K., and Kromer, B.: Possible solar origin of the 1,470-year glacial climate cycle demonstrated in a coupled model, Nature, 438, 208–211, 2005.

Broecker, W. S., Bond, G., Klas, M., Bonani, G., and Wolfli, W.: A salt oscillator in the glacial Atlantic? The concept, Paleoceanography, 5, 469–477, 1990.

Capron, E., Landais, A., Chappellaz, J., Schilt, A., Buiron, D., Dahl-Jensen, D., Johnsen, S. J., Jouzel, J., Lemieux-Dudon, B., Loulergue, L., Leuenberger, M., Masson-Delmotte, V., Meyer, H., Oerter, H., and Stenni, B.: Millennial and sub-millennial scale climatic variations recorded in polar ice cores over the last glacial period, Clim. Past, 6, 345–365, doi:10.5194/cp-6-345-2010, 2010.

Casty, C., Wanner, H., Luterbacher, J., Esper, J., and Böhm, R.: Temperature and precipitation variability in the European Alps since 1500, Int. J. Climatol., 25, 1855–1880, 2005.

Cheng, H., Edwards, R. L., Wang. X., Woodhead, J., Hellstrom, J., Wang, Y. J., and Kong, X. G.: A new generation of ^{230}Th dating techniques: Tests of precision and accuracy, Goldschmidt Conference Abstracts, Geochim. Cosmochim. Ac., A157, 2008.

Cheng, H., Edwards, R. L., Broecker, W. S., Denton, G. H., Kong, X., Wang, Y., Zhang, R., and Wang, X.: Ice Age terminations, Science, 326, 248–252, 2009.

Clark, P. U., Marshall, S. J., Clarke, G. K. C., Hostetler, S. W., Licciardi, J. M., and Teller, J. T.: Freshwater forcing of abrupt climate change during the Last Glaciation, Science, 293, 283–287, 2001.

Claussen, M., Ganopolski, A., Brovkin, V., Gerstengarbe, F.-W., and Werner, P.: Simulated global-scale response of the climate system to Dansgaard/Oeschger and Heinrich events, Clim. Dynam., 21, 361–370, 2003.

Clement, A. C. and Cane, M. A.: A role for the tropical Pacific coupled ocean-atmosphere system on Milankovitch and millennial timescales. Part I: A modelling study of tropical Pacific variability, in: Mechanisms of global climate change at millennial time scales, edited by: Geophys. Monogr. Ser., 112, edited by: P. U. Clark, Webb, R. S., and Keigwin, L. D., AGU, Washington D. C., 363–371, 1999.

Clement, A. C. and Peterson, L. C.: Mechanisms of abrupt climate change of the Last Glacial period, Rev. Geophys., 46, RG4002, doi:10.1029/2006RG000204, 2008.

Cruz, F. W., Karmann, I., Viana, O. Jr., Burns, S. J., Ferrari, J. A., Vuille, M., Sial, A. N., and Moreira, M. Z.: Stable isotope study of cave percolation waters in subtropical Brazil: Implications for paleoclimate inferences from speleothems, Chem. Geol., 220, 245–262, 2005.

Dansgaard, W., Johnsen, S. J., Clausen, H. B., Dahl-Jensen, D., Gundestrup, N. S., Hammer, C. U., Hvidberg, C. S., Steffensen, J. P., Sveinbjörnsdottir, A. E., Jouzel, J., and Bond, G.: Evidence for general instability of past climate from a 250-kyr ice-core record, Nature, 364, 218–220, 1993.

Ditlevsen, P. D. and Johnsen, S. J.: Tipping points: Early warning and wishful thinking, Geophys. Res. Lett., 37, L19703, doi:10.1029/2010GL044486, 2010.

Drysdale, R. N., Zanchetta, G., Hellstrom, J. C., Fallick, A. E., McDonald, J., and Cartwright, I.: Stalagmite evidence for the precise timing of North Atlantic cold events during the early last glacial, Geology, 35, 77–80, 2007.

Dykoski, C. A., Edwards, R. L., Cheng, H., Yuan, D., Cai, Y., Zhang, M., Lin, Y., Qing, J., An, Z., and Revenaugh, J.: A high-resolution, absolute-dated Holocene and deglacial Asian monsoon record from Dongge Cave, China, Earth Planet. Sci. Lett., 233, 71–86, 2005.

Edwards, R. L., Chen, J. H., and Wasserburg, G. J.: ^{238}U-^{234}U-^{230}Th-^{232}Th systematics and the precise measurement of time over the past 500,000 years, Earth Planet. Sci. Lett., 81, 175–192, 1986.

Fleitmann, D., Cheng, H., Badertscher, S., Edwards, R. L., Mudelsee, M., Göktürk, O. M, Fankhauser, A., Pickering, R., Raible, C. C., Matter, A., Kramers, J., and Tüysüz, O.: Timing and climatic impact of Greenland interstadials recorded in stalagmites from northern Turkey, Geophys. Res. Lett., 36, L19707, doi:10.1029/2009GL040050, 2009.

Friedman, I. and O'Neil, J. R.: Compilation of stable isotope fractionation factors of geochemical interest, U.S. Geological Survey Professional Paper 440-KK, Data of Geochemistry, 6th Edn, 1977.

Ganopolski, A. and Rahmstorf, S.: Abrupt glacial climate changes due to stochastic resonance, Phys. Rev. Lett., 88, 038501-1–038501-4, doi:10.1103/PhysRevLett.88.038501, 2002.

Genty, D., Blamart, D., Ouahdi, R., Gilmour, M., Baker, A., Jouzel, J., and Van-Exter, S.: Precise dating of Dansgaard-Oeschger climate oscillations in western Europe from stalagmite data, Nature, 421, 833–837, 2003.

Grachev, A. M., Brook, E. J., and Severinghaus, J. P.: Abrupt changes in atmospheric methane at the MIS 5b-5a transition, Geophys. Res. Lett., 34, L20703, doi:10.1029/2007GL029799, 2007.

Grootes, P. M. and Stuiver, M.: Oxygen 18/16 variability in Greenland snow and ice with 10^{-3}- to 10^5-year time resolution, J. Geophys. Res., 102, 26455–26470, 1997.

Grootes, P. M., Stuiver, M., White, J. W. C., Johnsen, S., and Jouzel, J.: Comparison of oxygen isotope records from the GISP2 and GRIP Greenland ice cores, Nature, 366, 552–554, 1993.

Huber, C., Leuenberger, M., Spahni, R., Flückiger, J., Schwander, J., Stocker, T.F., Johnsen, S., Landais, A., and Jouzel, J.: Isotope calibrated Greenland temperature record over Marine Isotope Stage 3 and ist relation to CH_4, Earth Planet. Sci. Lett., 243, 504–519, 2006.

Humer, G., Rank, D., Trimborn, P., and Stichler, W.: Niederschlagsisotopenmessnetz Österreich, Monographien, Vol. 52, Umweltbundesamt, Vienna, 86 pp., 1995.

IAEA/WMO: Global Network of Isotopes in Precipitation, The GNIP database, accessible at: http://isohis.iaea.org, last access: 23 November, 2010.

Johnsen, S. J., Dahl-Jensen, D., Gundestrup, N., Steffensen, J. P., Clausen, H. B., Miller, H., Masson-Delmotte, V., Sveinbjörnsdottir, A. E., and White, J.: Oxygen isotope and palaeotemperature records from six Greenland ice-core stations: Camp Century, Dye-3, GRIP, GISP2, Renland and NorthGRIP, J. Quaternary Sci., 16, 299–307, 2001.

Kaiser, A., Scheifinger, H., Kralik, M., Papesch, W., Rank, D., and Stichler, W.: Links between meteorological conditions and spatial/temporal variations in long-term isotope records from the Austrian Precipitation Network, in: C&SPaperSeries 13/P, International Conference "Study of Environmental Change using isotope techniques", IAEA, Vienna, 23–27 April 2001, 67–77, 2001.

Kim, S. T. and O'Neil, J. R.: Equilibrium and nonequilibrium oxygen isotope effects in synthetic carbonates, Geochim. Cosmochim. Ac., 61, 3461–3475, 1997.

Lachniet, M. S.: Climatic and environmental controls on speleothem oxygen-isotope values, Quaternary Sci. Rev., 28, 412–432, 2009.

Lambeck, K. and Chappell, J.: Sea level change through the last glacial cycle, Science, 292, 679–686, 2001.

Lang, C., Leuenberger, M., Schwander, J., and Johnsen, S.: 16°C rapid temperature variation in Central Greenland 70,000 years ago, Science, 286, 934–937, 1999.

Laskar, J., Robutel, P., Joutel, F., Gastineau, M., Correia, A. C. M., and Levrard, B.: A long-term numerical solution for the insolation quantities of the Earth, Astron. Astrophys., 428, 261–285, 2004.

Loulergue, L., Schilt, A., Spahni, R., Masson-Delmotte, V., Blunier, T., Lemieux, B., Barnola, J.-M., Raynaud, D., Stocker, T. F., and Chappellaz, J.: Orbital and millennial-scale features of atmospheric CH_4 over the past 800,000 years, Nature, 453, 383–386, 2008.

Lowe, J. J., Rasmussen, S. O., Björck, S., Hoek, W. Z., Steffensen, J. P., Walker, M. J. C., Yu, Z. C., and the INTIMATE group: Synchronisation of palaeoenvironmental events in the North Atlantic region during the Last Termination: a revised protocol recommended by the INTIMATE group, Quaternary Sci. Rev., 27,

6–17, 2008.

Meese, D. A., Gow, A. J., Alley, R. B., Grootes, P. M., Ram, M., Taylor, K. C., Zielinski, G. A., Bolzan, J. F., Mayewski, P. A., and Waddington, E. D.: The Greenland Ice Sheet Project 2 depth-age scale: Methods and results, J. Geophys. Res., 102, 26411–26423, 1997.

North Greenland Ice Core Project members: High-resolution record of Northern Hemisphere climate extending into the last interglacial period, Nature, 431, 147–151, 2004.

Paillard, D., Labeyrie, L., and Yiou, P.: Macintosh program performs time-series analysis, Eos Trans. AGU, 77, 379, doi:10.1029/96EO00259, 1996.

Peavoy, D. and Franzke, C.: Bayesian analysis of rapid climate change during the last glacial using Greenland ?18O data, Clim. Past, 6, 787–794, doi:10.5194/cp-6-787-2010, 2010.

R Development Core Team: The R Project for Statistical Computing, accessible at: http://www.r-project.org, last access: 23 November, 2010.

Rahmstorf, S.: Ocean circulation and climate during the past 120,000 years, Nature, 419, 207–214, 2002.

Rahmstorf, S.: Timing of abrupt climate change: a precise clock, Geophys. Res. Lett., 30, 1510, doi:10.1029/2003GL017115, 2003.

Richards, D. A. and Dorale, J. A.: Uranium series chronology and environmental applications of speleothems, in: Uranium series geochemistry, edited by: Bourdon, B., Henderson, G. M., Lundstrom, C. C., Turner, S., Rev. Mineral. Geochem., 52, 407–460, 2003.

Rousseau, D.-D., Kukla, J., and McManus, J.: What is what in the ice and the ocean?, Quaternary Sci. Rev., 25, 2025–2030, 2006.

Rozanski, K., Araguas-Araguas, L., and Gonfiantini, R.: Relation between long-term trends of oxygen-18 isotope composition of precipitation and climate, Science, 258, 981–985, 1992.

Schmittner, A. and Galbraith, E. D.: Glacial greenhouse-gas fluctuations controlled by ocean circulation changes, Nature, 456, 373–376, 2008.

Scholz, D. and Hoffmann, D.: StalAge – an algorithm designed for construction of speleothem age models, Quat. Geochronol., 6, 369–382, 2011.

Severinghaus, J. P., Sowers, T., Brook, E. J., Alley, R. B., and Bender, M. L.: Timing of abrupt climate change at the end of the Younger Dryas interval from thermally fractionated gases in Polar ice, Nature, 391, 141–146, 1998.

Shen, C.-C., Li, K.-S., Sieh, K., Natawidjaja, D., Cheng, H., Wang, X., Edwards, R. L., Lam, D. D., Hsieh, Y.-T., Fan, T.-Y., Meltzner, A. J., Taylor, F. W., Quinn, T. M., Chiang, H.-W., and Kilbourne, K. H.: Variation of initial $^{230}Th/^{232}Th$ and limits of high precision U-Th dating of shallow-water corals, Geochim. Cosmochim. Ac., 72, 4201–4223, 2008.

Sodemann, H. and Zubler, E.: Seasonal and inter-annual variability of the moisture sources for Alpine precipitation during 1995–2002, Int. J. Climatol., 30, 947–961, 2010.

Spötl, C. and Mangini, A.: Stalagmite from the Austrian Alps reveals Dansgaard-Oeschger events during isotope stage 3: Implications for the absolute chronology of Greenland ice cores, Earth Planet. Sci. Lett., 203, 507–518, 2002.

Spötl, C. and Vennemann, T. W.: Continuous-flow isotope ratio mass spectrometric analysis of carbonate minerals, Rapid Commun. Mass Sp., 17, 1004–1006, 2003.

Spötl, C., Mangini, A., and Richards, D. A.: Chronology and pale-oenvironment of Marine Isotope Stage 3 from two high-elevation speleothems, Austrian Alps, Quaternary Sci. Rev., 25, 1127–1136, 2006.

Spötl, C., Nicolussi, K., Patzelt, G., Boch, R., and DAPHNE Team: Humid climate during deposition of sapropel 1 in the Mediterranean Sea: Assessing the influence on the Alps, Global Planet. Change, 71, 242–248, 2010.

Steffensen, J. P., Andersen, K. K., Bigler, M., Clausen, H. B., Dahl-Jensen, D., Fischer, H., Goto-Azuma, K., Hansson, M., Johnsen, S. J., Jouzel, J., Masson-Delmotte, V., Popp, V., Rasmussen, S. O., Röthlisberger, R., Ruth, U., Stauffer, B., Siggaard-Andersen, M.-L., Sveinbjörnsdóttir, A. E., Svensson, A., White, J. W. C.: High-resolution Greenland ice core data show abrupt climate change happens in few years, Science, 321, 680–684, 2008.

Svensson, A., Andersen, K. K., Bigler, M., Clausen, H. B., Dahl-Jensen, D., Davies, S. M., Johnsen, S. J., Muscheler, R., Parrenin, F., Rasmussen, S. O., Rthlisberger, R., Seierstad, I., Steffensen, J. P., and Vinther, B. M.: A 60 000 year Greenland stratigraphic ice core chronology, Clim. Past, 4, 47–57, doi:10.5194/cp-4-47-2008, 2008.

Von Grafenstein, U., Erlenkeuser, H., Brauer, A., Jouzel, J., and Johnsen, S. J.: A mid-European decadal isotope-climate record from 15,000 to 5000 years B. P., Science, 284, 1654–1657, 1999.

Wang, X., Auler, A. S., Edwards, R. L., Cheng, H., Ito, E., Wang, Y., Kong, X., and Solheid, M.: Millennial-scale precipitation changes in southern Brazil over the past 90,000 years, Geophys. Res. Lett., 34, L23701, doi:10.1029/2007GL031149, 2007.

Wang, Y. J., Cheng, H., Edwards, R. L., An, Z. S., Wu, J. Y., Shen, C.-C., and Dorale, J. A.: A high-resolution absolute dated late Pleistocene monsoon record from Hulu Cave, China, Science, 294, 2345–2348, 2001.

Wang, Y. J., Cheng, H., Edwards, R. L., Kong, X., Shao, X., Chen, S., Wu, J., Jiang, X., Wang, X., and An, Z.: Millennial- and orbital-scale changes in the East Asian monsoon over the past 224,000 years, Nature, 451, 1090–1093, 2008.

Wolff, E. W., Chappellaz, J., Blunier, T., Rasmussen, S. O., and Svensson, A.: Millennial-scale variability during the last glacial: The ice core record, Quaternary Sci. Rev., 29, 2828–2838, 2010.

Wunsch, C.: Abrupt climate change: An alternative view, Quaternary Res., 65, 191–203, 2006.

Xia, Z., Kong, X., Jiang, X., and Cheng, H.: Precise dating of East-Asian-Monsoon D/O events during 95-56 ka BP: Based on stalagmite data from Shanbao Cave at Shennongjia, China, Sci. China Ser. D, 50, 228–235, 2007.